Magnetic properties of $(Nd,Ca)(Ba,La)Co_2O_{5+\delta}$ tuned by the site-selected charge doping, oxygen disorder, and hydrostatic pressure

J. Pietosa,[1] S. Kolesnik,[2] R. Puzniak,[1] A. Wisniewski,[1] B. Poudel,[2] and B. Dabrowski[2]
[1]*Institute of Physics, Polish Academy of Sciences, Aleja Lotnikow 32/46, PL-02668 Warsaw, Poland*
[2]*Department of Physics, Northern Illinois University, De Kalb, Illinois 60115, USA*
(Received 25 April 2017; revised manuscript received 11 September 2017; published 10 November 2017)

Comprehensive study of magnetic properties of the layer-ordered perovskites $Nd_{1-x}Ca_xBa_{1-y}La_yCo_2O_{5+\delta}$ is presented as a function of the site-selected charge doping [$c = (x-y)/2 + \delta - 0.5$, $x \leqslant 0.2$ and $y \leqslant 0.1$, $0.07 < \delta < 0.84$], oxygen disorder, and hydrostatic pressure $P < 10$ kbar. The single-phase oxygen-ordered orthorhombic phase exhibiting complex ferrimagnetic, antiferromagnetic, and metal-insulator phase transitions was found for a narrow oxygen range around $\delta \sim 0.5 \pm 0.1$. Significant difference between impact of hole ($c > 0$) and electron ($c < 0$) doping was observed depending on the site of cation substitution. Gradual enhancement of the Curie temperature T_C was observed over the whole range of c to be unaffected by the local oxygen vacancy disorder. Maximum of the Néel temperature T_N at $c = 0$ was found rapidly disappearing at $c = 0.05$ for Ca/Nd substitution while it was maintained for La/Ba substitution, indicating that the oxygen vacancy disorder, especially for $\delta > 0.5$, has a larger effect on antiferromagnetic phase than the charge doping. The temperature of metal-insulator transition T_{MIT} was found practically unchanged by either charge doping or disorder. The application of hydrostatic pressure slightly suppressed T_C and increased T_N by stabilization of the antiferromagnetic phase with the largest observed value of $dT_N/dP = 5.75$ K/kbar. Complex magnetic behavior affected by hydrostatic pressure was accounted for by ferro- and antiferromagnetic interactions resulting from the charge separation and spin transitions.

DOI: 10.1103/PhysRevMaterials.1.064404

I. INTRODUCTION

The layered-ordered orthorhombic perovskite cobaltites $RBaCo_2O_{5+\delta}$ (R = lanthanide ion or Y) exhibit a striking sequence of complex magnetic and electronic phase transitions for $\delta = 0.5$. With increasing temperature, the transitions depend on the ionic size of R: antiferromagnet-ferromagnet ($T_N = 200$–250 K), ferromagnet-paramagnet ($T_C = 280$–310 K), and insulator-metal ($T_{MIT} = 330$–360 K). In addition, these transitions can be tuned by a wide range of substitutions at the R-, Ba-, and Co sites or by a change of the oxygen content $5+\delta$, which bring charge doping and structural changes [1–5]. The layered structure [3], which was initially studied by the change of the oxygen content around $\delta = 0.5$, consists of the aligned sheets of $RO_\delta - CoO_2 - BaO - CoO_2$ along the c axis [4]. The Co ions are coordinated by 5 or 6 oxygen ions forming a 2-dim corner-shared network of square-based pyramids and octahedra. The variation of δ alters charge doping of the CoO_2 planes and, more importantly, leads to the insertion or removal of oxygen ions in the RO_δ planes, changing the ratio of the octahedral to pyramidal Co coordination, i.e., controls the coupling between CoO_2 planes along the c axis. For $\delta = 0$, i.e., for the compound with no oxygen in the RO_δ layers, all Co ions are pyramidally coordinated (CoO_5), which results in isolated network of double Co-O planes sharing oxygen ion in the BaO layer. Increase of δ up to 1 leads to a transition to octahedral coordination of all Co ions (CoO_6) forming 3-dim perovskite network. For the compound with $\delta = 0.5$, there is an additional oxygen vacancy order resulting in single planes of octahedrally coordinated CoO_6, coupled by the double chains of pyramidally coordinated CoO_5 along the b axis, and the partially coupled double-Co-O planes along the c axis. The oxygen vacancy order produces orthorhombic crystal structure $Pmmm$ with two and four Co sites above and below T_{MIT} due to the Co spin ordering at T_{MIT} [1–6], while only Co^{3+} ions are present at all crystal sites [4]. Variation of δ near 0.5 leads to the changes in the formal valence of $Co^{(3+c)+}$ ($c = \delta - 0.5$) ions; the hole doping ($c > 0$ for $\delta > 0.5$) or electron doping ($c < 0$ for $\delta < 0.5$) and, in addition, to a disturbance of the oxygen vacancy ordering along the b axis. Taskin *et al.* [4] have shown that any deviation from optimal charge doping of the Co^{3+} ion ($c \neq 0$ for $\delta \neq 0.5$) leads to a decrease in critical temperatures of all observed phase transitions. Specifically, the T_{MIT} was very slightly suppressed on the electron-doped side ($c < 0$) and little more on the hole-doped side ($c > 0$). The T_C and T_N showed symmetric small and large suppression, respectively, on both sides. Moreover, the magnetic and transport properties pointed to the phase separation into two insulating phases in the electron-doped region ($c < -0.05$) and into the insulating and metallic phases in the hole-doped region ($c > 0.05$) when δ was below 0.45 and beyond 0.55, respectively. Thus, the range of $0.45 < \delta < 0.55$ establishes a narrow single-phase charge-doped region ($-0.05 < c < 0.05$) of the oxygen vacancy ordered orthorhombic phase [4].

Another method of a simpler charge doping was studied by heterovalent substitutions at the R, Ba, and Co sites for fixed $\delta = 0.5$, which maintained the oxygen vacancy ordering, i.e., it does not affect the ratio of the pyramidal and octahedral coordinations of cobalt and the vacancy ordering along the b axis [5,7–9]. These substitutions established a somewhat different phase diagram of the electronic and magnetic transitions than by the variation of δ, for example, in the case of the $Nd^{3+}{}_{1-x}Ca^{2+}{}_xBaCo^{(3+x/2)+}{}_2O_{5.5}$ system, for which a wider single-phase orthorhombic hole-doping range $c = x/2 = 0$–0.1 was achieved [5]. The value of T_{MIT} was very slightly and linearly lowered from 345 to 340 K for c varying between 0 and 0.1. The T_C showed linear increase

from 260 to 340 K for c increasing from 0 to 0.08 ($x = 0.16$), where the T_C merged with the T_{MIT}. The T_N was rapidly suppressed with increasing c, and for $c \geqslant 0.05$ ($x \geqslant 0.1$) the antiferromagnetic (AFM) phase disappeared [5]. Application of hydrostatic pressure restored the AFM phase for $c = x/2 =$ 0–0.06. Even more pronounced enhancement of T_N with a simultaneous decrease of the T_C was shown for the larger $c = 0.03$ hole doping [10]. The absence of the AFM order in $Nd_{0.9}Ca_{0.1}BaCo_2O_{5.5}$ has been found to remain unchanged by applying a hydrostatic pressure up to 10 kbar [11].

Our recent work on selected double substituted at the Nd site and on oxygen content $5+\delta$ varied $Nd_{1-x}Ca_xBaCo_2O_{5+\delta}$ ($c = x/2 + \delta - 0.5$), has reported at ambient pressure the reappearance of the AFM phase, caused by an increase of δ above 0.51 for $x = 0.1$ ($c = 0.06$). For the samples with $\delta = 0.52$ and 0.59 ($c = 0.07$ and 0.14), a coexistence of a well-developed AFM phase with the ferrimagnetic one was observed [11]. We have also investigated the heterovalent La for Ba substituted $Nd^{3+}Ba^{2+}{}_{1-y}La^{3+}{}_yCo_2O_{5+\delta}$ ($y = 0.06$) with a range of the effective charge doping $c = -y/2 + \delta -$ 0.5 ($\delta = 0.26$–0.90) in order to probe separately the effects of the charge doping and the disruption of the oxygen vacancy ordering [12]. The insulator-to-metal transition temperature T_{MIT} and the Néel temperature T_N have reached maximum values for the slightly electron doped sample $c = -0.03$ with a perfect oxygen ordering $\delta = 0.5$, while the Curie temperature T_C has shown continuous decrease with the increase of δ from 265 to 195 K ($-0.07 < c < 0.13$). Comparison of the magnetic ac and dc measurements for the oxygen-doped $GdBaCo_2O_{5+\delta}$ [4] and the Ca-substituted $NdBaCo_2O_{5.5}$ [5] systems has revealed that the perfection of the oxygen ordering is more important in controlling the magnetic properties than the overall charge doping. The hydrostatic pressure was observed to stabilize the AFM phase for both systems of $NdBa_{0.94}La_{0.06}Co_2O_{5.5}$ [12] and $Nd_{0.94}Ca_{0.06}BaCo_2O_{5.5}$ [10].

In this paper, we present a phase diagram of the striking magnetic and resistive properties of the $Nd_{1-x}Ca_xBa_{1-y}La_yCo_2O_{5+\delta}$ system achievable over the full range of structurally ordered orthorhombic phase. When the charge doping by the cation substitutions and by the variation of oxygen content δ are treated on equal footing, the achieved charge doping are $c = -0.19$ to 0.42, -0.21 to 0.43, -0.5 to 0.27 (from Ref. [4]), -0.13 to 0.37, and -0.38 to 0.31 for $y = 0.1$, $y = 0.06$, $y = x = 0$, $x = 0.06$, and $x = 0.10$, respectively. The results of magnetic study as a function of the effective charge doping c show that in addition to the observation that the perfection of the oxygen ordering is more important in controlling the magnetic properties than the overall charge doping, the site substitutions of x and y do not lead to exactly the same properties at the same c and δ. This comes from the fact that in Ba layers, oxygen atoms fully occupy their crystallographic sites, whereas significant vacancies and oxygen vacancy ordering takes place in Nd layers (Fig. 1).

We show gradual enhancement of the ferrimagnetic phase, starting from the electron doping region ($NdBa_{1-y}La_yCo_2O_{5.5}$) to the hole-doped one ($Nd_{1-x}Ca_xBaCo_2O_{5.5}$), when pyramidal and octahedral coordinations are preserved ($\delta = 0.5$). Also, it is observed that the AFM phase does not disappear for $NdBa_{0.9}La_{0.1}Co_2O_{5.5}$, contrary to $Nd_{0.9}Ca_{0.1}BaCo_2O_{5.5}$ [5]

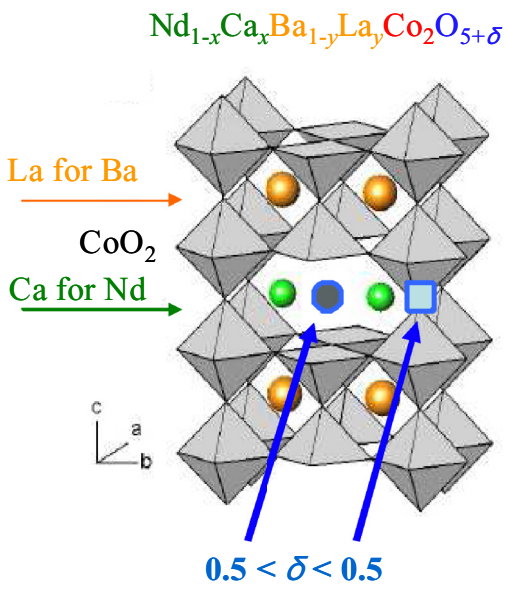

FIG. 1. Crystal structure of $Nd_{1-x}Ca_xBa_{1-y}La_yCo_2O_{5+\delta}$.

with the same c equal to 0.05. The possibility of charge doping by oxygen content variation in $Nd_{0.9}Ca_{0.1}BaCo_2O_{5+\delta}$ has led to pressure-induced appearance of AFM phase in $Nd_{0.9}Ca_{0.1}BaCo_2O_{5.45}$.

II. EXPERIMENTAL DETAILS

Polycrystalline samples of (Nd,Ca)(Ba,La)$Co_2O_{5+\delta}$ have been obtained by using a standard solid-state synthesis method described in detail in Ref. [5]. Four series of $Nd_{0.9}Ca_{0.1}BaCo_2O_{5+\delta}$, $Nd_{0.94}Ca_{0.06}BaCo_2O_{5+\delta}$, $NdBa_{0.94}La_{0.06}Co_2O_{5+\delta}$, and $NdBa_{0.9}La_{0.1}Co_2O_{5+\delta}$ samples with different oxygen contents varying from 5.07 to 5.9 were synthesized by annealing in argon or oxygen at temperatures 250–800 °C or under high pressure of oxygen (~ 200 bar O_2 at 450–500 °C). X-ray diffraction patterns were collected using a Rigaku diffractometer. Magnetic measurements were carried out using a Magnetic Property Measurement System (MPMS, Quantum Design). Hydrostatic pressure was applied, using an easyLab Technologies MCell10 pressure cell with Daphne 7373 oil [13,14]. A high-purity Sn wire (0.25 mm in diameter) was employed as an *in situ* manometer.

III. RESULTS AND DISCUSSION

A. Structural properties of $Nd_{1-x}Ca_xBa_{1-y}La_yCo_2O_{5+\delta}$

X-ray diffractograms obtained in the range $2\theta = 30$–50° were refined using crystallographic data analysis software (GSAS). The crystal structure of most of the samples was analyzed within either an orthorhombic *Pmmm* phase (with arrangement of lattice parameters of the $a_p \times 2a_p \times 2a_p$ type, where a_p is the lattice parameter of a simple perovskite) or a tetragonal *P4/mmm* phase ($a_p \times a_p \times 2a_p$). Lattice parameters obtained from refinements are presented in Figs. 2(a)–2(d). The orthorhombic phase, characterized by ordering of alternating CoO_5 pyramids and CoO_6

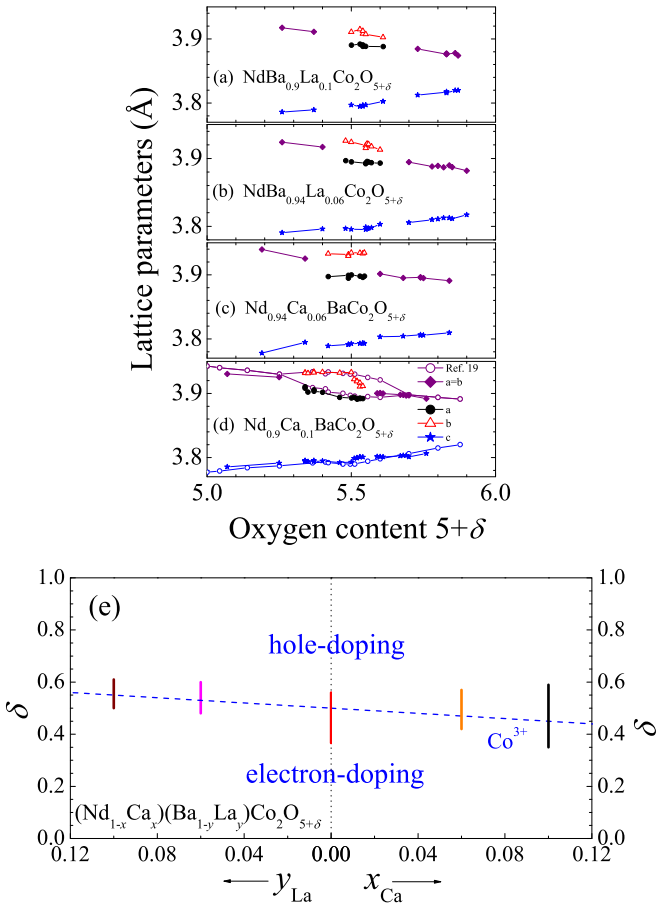

FIG. 2. Lattice parameters as a function of oxygen content for $NdBa_{0.9}La_{0.1}Co_2O_{5+\delta}$ (a), $NdBa_{0.94}La_{0.06}Co_2O_{5+\delta}$ (b), $Nd_{0.94}Ca_{0.06}Co_2O_{5+\delta}$ (c), and $Nd_{0.9}Ca_{0.1}BaCo_2O_{5+\delta}$ (d). Open symbols are lattice parameters for $NdBaCo_2O_{5+\delta}$ crystals from Ref. [15]. Panel (e) shows the range of oxygen index (marked by solid lines) associated with crystallization in the *Pmmm* space group. The data for $NdBaCo_2O_{5+\delta}$ (red line at the center of the figure) are taken from Ref. [15].

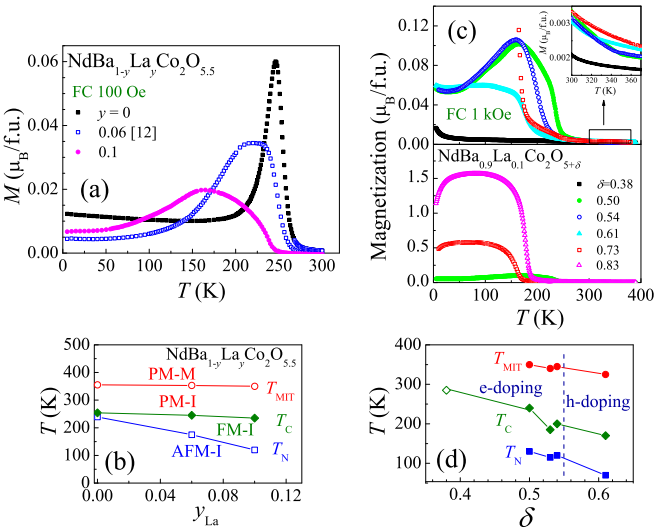

FIG. 3. (a) Temperature dependences of magnetization for $NdBa_{1-y}La_yCo_2O_{5.5}$ with $y = 0$, 0.06, and 0.1. (b) Phase diagram in which PM-M is the paramagnetic metallic phase, PM-I is the PM insulating phase, FM-I is the ferrimagnetic insulating phase, and AFM-I is the AFM insulating phase. The main transition temperatures T_{MIT}, T_C, and T_N are plotted. (c) Temperature dependences of magnetization for $NdBa_{0.9}La_{0.1}Co_2O_{5+\delta}$ with selected oxygen contents. Inset shows the same data in the vicinity of T_{MIT}. Panel (d) shows oxygen content dependence of main transition temperatures T_N, T_C, and T_{MIT} for $NdBa_{0.9}La_{0.1}Co_2O_{5+\delta}$. Closed symbols refer to the transitions in orthorhombic phase, while the open symbols refer to the transitions beyond orthorhombic phase.

octahedra, was found for a restricted range of δ near 0.5. Outside of that oxygen content range, the materials adopt the tetragonal structure. Similar behavior was observed for $NdBaCo_2O_{5+\delta}$ crystals [15]. Figure 2(e) shows the range of oxygen stoichiometry where the single-phase orthorhombic samples were found, which are the focus of this study. The range depends on the cation substitution level and extends from $5 + \delta = 5.34$–5.59 for $Nd_{0.9}Ca_{0.1}BaCo_2O_{5+\delta}$ to ~ 5.5–5.61 for $NdBa_{0.9}La_{0.1}Co_2O_{5+\delta}$, i.e., it is significantly narrower for the La for Ba substituted samples.

B. Magnetic properties of $Nd_{1-x}Ca_xBa_{1-y}La_yCo_2O_{5+\delta}$

Figure 3(a) presents temperature dependences of magnetization measured at ambient pressure, using a field-cooling procedure in a magnetic field of 0.1 kOe, for $NdBa_{1-y}La_yCo_2O_{5.5}$ with $y = 0$, 0.06, and 0.1. The characteristic temperatures determined from the $M(T)$ dependences are presented in Fig. 3(b). The values of T_N and T_C in this study were determined from the maximum of absolute value of derivative dM_{FC}/dT. Upon electron doping by La substitution, the value of T_N decreases precipitately from 245 K for $y = 0$ to 120 K for $y = 0.1$. This decrease is however slower than that for the hole-doped $Nd_{0.9}Ca_{0.1}BaCo_2O_{5.5}$ [5] and for the isovalent substitution in $YBa_{0.9}Ca_{0.1}Co_2O_{5.5}$ [6,16]. The AFM phase is thus suppressed upon all kinds of substitutions at the *R*- and Ba sites. The value of T_C also decreases in $NdBa_{1-y}La_yCo_2O_{5.5}$ but much slower than T_N. This is in contrast to increasing T_C observed for the hole-doped $(Nd,Ca)BaCo_2O_{5.5}$ [5] but similar to behavior observed for isoelectronic $Y(Ba,Ca)Co_2O_{5.5}$ [6,16]. Kolesnik *et al.* have associated the increase in T_C for $(Nd,Ca)BaCo_2O_{5.5}$ with the *p*-type doping by Ca^{2+} for Nd^{3+} and creation of the Co^{3+} and Co^{4+} mixed-valence states [5]. Moreover, similar *p*-type doped increase of T_C, originating from Co^{3+}–O–Co^{4+} interactions, was observed in Ca-substituted compounds with different R^{3+} ions [17–19]. In the case of $Nd(Ba,La)Co_2O_{5.5}$, the decrease of T_C can be thus associated with electron doping, which creates Co^{2+} and Co^{3+} mixed-valence states favoring AFM superexchange interactions [20]. Since the magnetic moments of Co^{3+} and Co^{2+} are different, the AFM coupling between Co^{3+} and Co^{2+} is expected to lead to the appearance of uncompensated magnetic moment. Such a doping, together with disproportion reaction for Co^{3+} [17], which reduces the importance the superexchange interaction through Co^{3+}–O–Co^{3+}, may be responsible for the decrease of T_N despite the more significant role of AFM coupling related to electron doping.

Figure 3(c) presents temperature dependences of magnetization for $NdBa_{0.9}La_{0.1}Co_2O_{5+\delta}$ with $\delta = 0.38$–0.83

measured at ambient pressure in magnetic field of 1 kOe using a field-cooling procedure. Both magnetic transitions at T_C and T_N are rather visible, so both anti- and ferrimagnetic phase fractions exist together in a broad δ range, as was already reported for the $GdBaCo_2O_{5+\delta}$ [4,15] and $PrBaCo_2O_{5+\delta}$ systems [21]. Also, the transition at T_{MIT} is clearly visible in magnetic measurements, as shown in the inset to Fig. 3(c). Increased doping by oxygen leads to a decrease of both T_C and T_N, and vanishing of the AFM phase fraction, which practically disappears near $\delta = 0.61$ [Fig. 3(d)]. Apparently, suppression of the AFM phase results from introducing Co^{4+} at the cost of Co^{2+}, such that ferromagnetic Co^{4+}/Co^{3+} interactions [20] become more important. This is manifested in $M(H)$ dependences measured at 80 K, in field-cooled (FC) mode, starting from $H = 50$ kOe (not shown). For $\delta = 0.5$, the value of magnetization recorded for $H = 50$ kOe is equal to $0.68\,\mu_B$/f.u., whereas for $\delta = 0.61$ it increases up to $0.93\,\mu_B$/f.u. Gradual hole doping by the change of oxygen content introduces not only Co^{4+} ions, but also disorders the Co–O network by formation of a larger number of CoO_6 octahedra at the expense of CoO_5 pyramids. This effect causes increasing delocalization of electrons across the Co–O–Co bonds and results in lowering T_C. Above $\delta = 0.61$, the oxygen vacancy ordering has mostly vanished as evidenced by sharp increase in magnetization below $T_C \sim 160$ K, typical for perovskite with random distribution of oxygen vacancies. A gradual decrease of magnetization at low temperatures indicates an appearance of antiferromagnetic ordering in ferromagnetic matrix, similar to that found for the $GdBaCo_2O_{5+\delta}$ system [4]. In the case of electron doping of $\delta = 0.38$ (in the range of tetragonal structure), the Co^{2+} ions content is increased at the cost of Co^{4+} ones. The Co^{3+}/Co^{2+} AFM coupling with ferrimagnetic features dominates the magnetic behavior of the sample. The value of T_C is equal to 285 K and the magnitude of magnetization continuously increases down to about 80 K, after which a vast increase of magnetization is observed, caused by paramagnetic contribution from Nd^{3+} ions [10]. The divergence between zero-field-cooled (ZFC) and FC curves indicates the presence of Co^{3+}/Co^{2+} clusters of the ferrimagnetic phase in the Co^{3+}/Co^{3+} AFM matrix [22].

C. Pressure dependence of magnetic properties of $NdBa_{1-y}La_yCo_2O_{5+\delta}$

It was reported for $NdBaCo_2O_{5.5}$ [10] that T_N and T_C increase under pressure. We have previously reported a more significant increase in T_N together with a decrease of T_C and a clear decrease in magnetization, explained as stabilization of the antiferromagnetic phase under pressure for La substitution at the Ba site at 6% and $\delta = 0.5$ [12]. At 10% of La substitution, the stabilization of the AFM phase is seen even more clearly. For all investigated slightly electron-doped samples with $\delta = 0.5$–0.54 [Figs. 4(a)–4(c)], we observe strong suppression of the ferrimagnetic state under pressure, evidenced by a striking decrease of magnetization. This enhancement of the antiferromagnetic phase under pressure is confirmed by magnetic hysteresis loops for $NdBa_{0.9}La_{0.1}Co_2O_{5+\delta}$, measured at 150 K, under ambient and hydrostatic pressure [see insets of Figs. 4(a)–4(c)]. All the hysteresis loops are typical of soft magnetic materials, characterized by rather weak hysteresis,

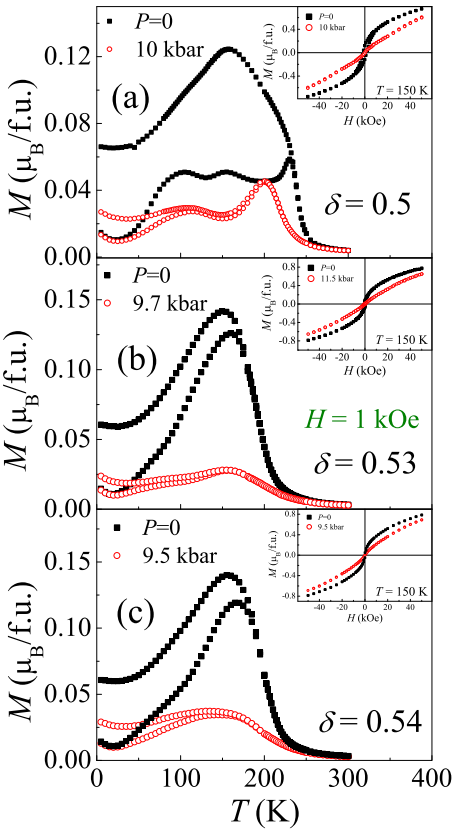

FIG. 4. Temperature dependences of ZFC and FC magnetization of $NdBa_{0.9}La_{0.1}Co_2O_{5+\delta}$ measured at 1 kOe for $\delta = 0.5$ (a), $\delta = 0.53$ (b), and $\delta = 0.54$ (c) at ambient and under hydrostatic pressure. Insets show magnetic field dependences of magnetization for $NdBa_{0.9}La_{0.1}Co_2O_{5+\delta}$ measured at 150 K, using the FC procedure in 50 kOe at ambient and under hydrostatic pressure.

which is suppressed under hydrostatic pressure. The loops do not reach saturation, supporting the model of Co^{2+}/Co^{3+} ferrimagnetic clusters dispersed in Co^{3+}/Co^{3+} AFM matrix for all investigated samples. The pressure variation of T_N and T_C can be well approximated by a linear dependence, as was shown in Refs. [10,12]. The linear coefficients of dT_N/dP and dT_C/dP for T_N and T_C, respectively, were determined by using the least-squares fitting method. For $NdBa_{1-y}La_yCo_2O_{5.5}$, a gradual enhancement of dT_N/dP was observed with an increase of y; $dT_N/dP = 1.03$ [10], 2.98 [12], and 5.75 K/kbar for $y = 0$, 0.06, and 0.10, respectively. For $y = 0.10$, upon hole doping by $0.5 < \delta < 0.54$ variation, the dT_N/dP decreases from 5.75 K/kbar for $\delta = 0.5$, through 1.16 K/kbar for $\delta = 0.53$ up to -5.72 K/kbar for $\delta = 0.54$.

It was shown for the hole doped system $(Nd,Ca)BaCo_2O_{5.5}$ that the increase of T_C observed at ambient conditions is suppressed under pressure. This behavior was explained by the usual ferromagnetic phase created by mixed valence of Co^{3+}/Co^{4+} ions [10]. For the electron-doped $NdBa_{1-y}La_yCo_2O_{5.5}$ system, a similar behavior is observed; $dT_C/dP = 0.62$ [12], -1.44, and -2.18 K/kbar for $x = 0$, 0.06, and 0.10, respectively. In electron-doped compounds, the mixed valence of Co^{2+}/Co^{3+} appears, giving rise to the Co^{2+}–O–Co^{3+} AFM coupling, ordered ferrimagnetically,

i.e., dependence of T_C under pressure in $Nd(Ba,La)Co_2O_{5+\delta}$ cannot be explained by formation of the usual ferromagnetic phase. It is difficult to correlate changes in magnetic properties with the average structural changes, since the lattice parameters are affected negligibly [Fig. 2(a)], despite the substitution of smaller La^{3+} (0.136 Å) for Ba^{2+} (0.161 Å) and oxygen content modification. Nevertheless, from a local structural point of view, ferrimagnetism arises when two ferromagnetic sublattices (of different magnitudes) couple antiferromagnetically along a particular direction or from the cooperative canting of AFM ordered magnetic moments. In order to keep the ferrimagnetic ordering, we should assume that Co^{3+} ion is, at least, in the intermediate spin state (IS, $t_{2g}^5 e_g^1$, $S = 1$) and Co^{2+} ion is in the low spin state (LS, $t_{2g}^6 e_g^1, S = \frac{1}{2}$). In that case, the observed suppression of ferrimagnetic ordering under pressure can be attributed to breaking of the magnetic coupling in the Co^{3+}–O–Co^{2+} chain, related to change of the spin state of some fraction of Co^{3+} ions from IS to LS, or change of the oxidation state of some fraction of Co^{2+} ions. Obviously, we cannot exclude modifications of spin states of Co^{3+} in the Co^{3+}–O–Co^{3+} network because magnetization measurements alone do not allow differentiation between these two fractions. In order to clarify the picture of pressure-induced suppression of ferrimagnetic ordering, the magnetic studies at pressures higher than 10 kbar would be required, since it is not obvious if the observed pressure-induced suppression would lead to a complete elimination of spontaneous ordering.

D. Magnetic properties of $Nd_{0.94}Ca_{0.06}BaCo_2O_{5+\delta}$

Earlier reports for $(Nd,Ca)BaCo_2O_{5.5}$ [5] and $Y(Ba,Ca)Co_2O_{5.5}$ [7] have shown a decrease of T_N as result of hole doping by iso- and hetero-electronic substitutions of calcium. To explain lowering T_N, the authors have considered several possibilities, mainly pointing to the expected size and charge disorder at the Ba and Nd sites, which may induce local oxygen disorder. To clarify the origin of lowering T_N, we studied the influence of the disorder on magnetic and electronic phases created intentionally by oxygen content modification in $Nd_{0.94}Ca_{0.06}Co_2O_{5+\delta}$ with fixed levels of Nd-Ca doping. Figure 5(a) presents the $M(T)$ dependences for $Nd_{0.94}Ca_{0.06}BaCo_2O_{5+\delta}$ with $\delta = 0.19$–0.60 ($c = -0.28$–0.13). The characteristic temperatures determined from the $M(T)$ curves are presented in Fig. 5(b). The highest $T_C = 285$ K for the orthorhombic phase is observed for $\delta = 0.5$ ($c = 0.03$) and decreases slowly to 265 K for $\delta = 0.54$ ($c = 0.07$), while it remains practically unchanged on the electron-doped side for $\delta = 0.42$ ($c = -0.05$). On the other hand, the highest $T_N = 152$ K for the orthorhombic phase is found for $\delta = 0.42$ at the high level of oxygen disorder, which favors electron-doped AFM and ferrimagnetic phases while the antiferromagnetic phase disappears for $\delta > 0.5$, similar to $Nd_{0.9}Ca_{0.1}BaCo_2O_{5.5}$ [5]. The change of T_{MIT} is quite small and similar to that of T_C, as it mainly depends on the perfection of oxygen ordering rather than on the overall charge doping. The collapse of oxygen vacancy ordering is observed by rapid decrease of magnetization in the hole-doped region ($\delta = 0.60$) and complete disappearance of spontaneous ordering ($\delta = 0.19$) [Fig. 5(a)].

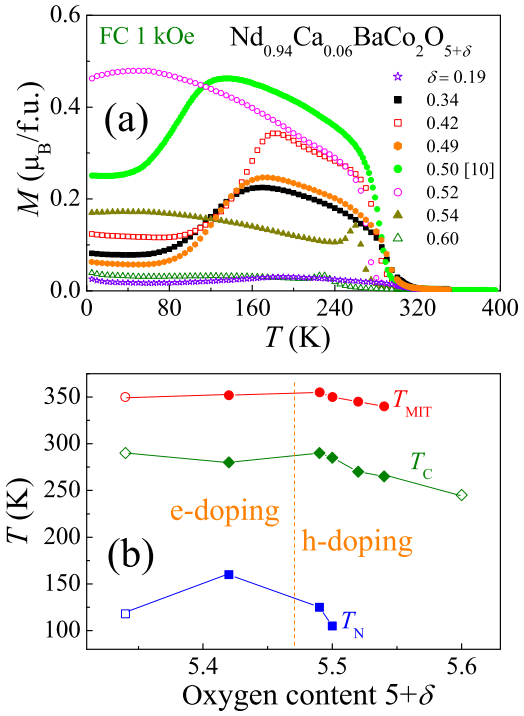

FIG. 5. Temperature dependences of magnetization for $Nd_{0.94}Ca_{0.06}BaCo_2O_{5+\delta}$ with selected oxygen contents (a). Panel (b) shows oxygen content dependence of main transition temperatures T_N, T_C, and T_{MIT} for $Nd_{0.94}Ca_{0.06}BaCo_2O_{5+\delta}$. Closed symbols refer to the transitions in orthorhombic phase, while the open symbols refer to the transitions beyond orthorhombic phase.

The importance of oxygen disorder is observed in the case of T_C and T_N. Hole doping of $Nd_{0.94}Ca_{0.06}BaCo_2O_{5+\delta}$ ($\delta = 0.47$–0.54) lowers T_C, despite an increased number of ferromagnetic Co^{3+}/Co^{4+} pairs [19], as evidenced by the increased value of magnetization for 50 kOe, from $\delta = 0.49$ (0.82 μ_B/f.u.) to $\delta = 0.54$ (1.02 μ_B/f.u.) [see the $M(H)$ loops recorded at ambient pressure, shown in the middle and lower panels of Fig. 6(b)]. On the other hand, the hole doping in case of Ca doping of $NdBaCo_2O_{5.5}$ [5] increased T_C. On the electron-doped side ($\delta = 0.42$–0.47), the value of T_C decreases slightly from 285 K for $\delta = 0.5$ to 280 K for $\delta = 0.42$ [Fig. 5(b)]. The presence of ferrimagnetic phase arises from increased content of Co^{3+}/Co^{2+} pairs coupled antiferromagnetically with effective ferrimagnetic ordering. As a result, we obtain the same situation as for $GdBaCo_2O_{5+\delta}$ [4]. The behavior of T_N for $Nd_{0.94}Ca_{0.06}BaCo_2O_{5+\delta}$ and $GdBaCo_2O_{5+\delta}$ [4] is different. For $GdBaCo_2O_{5+\delta}$ [4], the value of T_N is maximal for $\delta = 0.5$, i.e., for perfect oxygen order. It decreases regardless of charge doping in a narrow range of δ between 0.45 and 0.55. In our case, it is seen that disorder induced simultaneously by cation substitution and variation of oxygen content shifts the highest value of T_N to $\delta = 0.42$.

E. Pressure dependence of magnetic properties of $Nd_{0.94}Ca_{0.06}BaCo_2O_{5+\delta}$

We have reported in Ref. [10] the stabilization of antiferromagnetic phase under pressure for $Nd_{0.94}Ca_{0.06}BaCo_2O_{5.5}$ as evidenced by larger increase (when compared to that

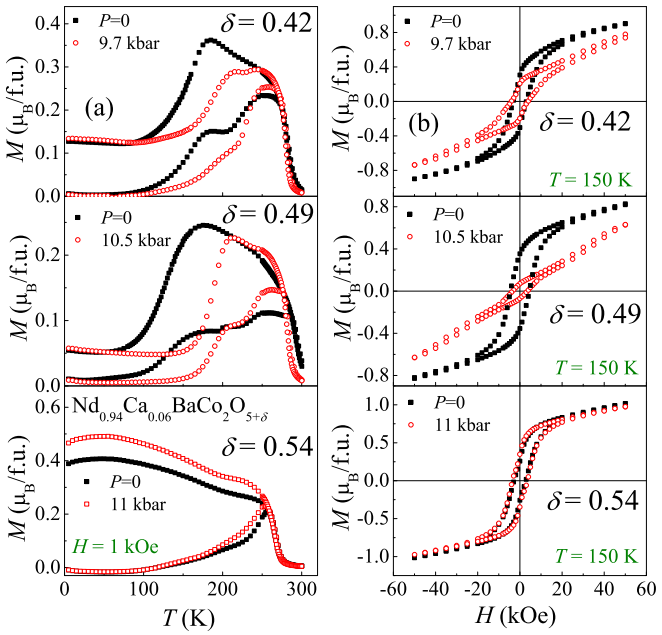

FIG. 6. Temperature dependences of ZFC and FC magnetization of $Nd_{0.94}Ca_{0.06}BaCo_2O_{5+\delta}$ measured at 1 kOe for selected δ index at ambient and under hydrostatic pressure (a). Panel (b) shows magnetic field dependences of magnetization for $Nd_{0.94}Ca_{0.06}BaCo_2O_{5+\delta}$ for selected δ index, measured using the FC procedure in 50 kOe at ambient and under hydrostatic pressure.

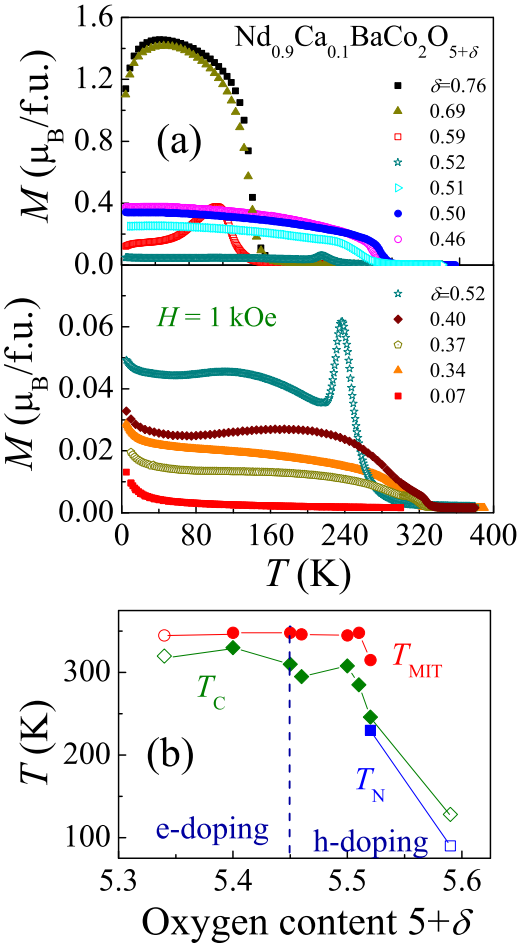

FIG. 7. (a) Temperature dependences of magnetization for $Nd_{0.9}Ca_{0.1}BaCo_2O_{5+\delta}$ with selected oxygen contents (after Ref. [11]). Panel (b) shows oxygen content dependence of main transition temperatures T_N, T_C, and T_{MIT} for $Nd_{0.9}Ca_{0.1}BaCo_2O_{5+\delta}$. Closed symbols refer to the transitions in orthorhombic phase, while the open symbols refer to the transitions beyond orthorhombic phase.

of pure $NdBaCo_2O_{5.5}$) of $dT_N/dP = 3.1(1)$ K/kbar together with a decrease of $dT_C/dP = -0.29(12)$ K/kbar. Decrease of T_C with increasing pressure was explained by the usual Co^{3+}–O–Co^{4+} ferromagnetic superexchange interactions with Co^{4+} ions appearing from hole doping [10]. The magnetic measurements under pressure, for weakly electron doped $Nd_{0.94}Ca_{0.06}BaCo_2O_{5.42}$ ($c = -0.02$) [Fig. 6(a), upper panel], revealed stabilization of the AFM phase, as for $Nd_{0.94}Ca_{0.06}BaCo_2O_{5.5}$, with the similar values of pressure coefficients: $dT_C/dP = -0.22(2)$ K/kbar and $dT_N/dP = 3.2(7)$ K/kbar. For $\delta = 0.49$ [Fig. 6(a), middle panel], with a fraction of Co^{4+} ($c = 0.05$) similar to that of $Nd_{0.94}Ca_{0.06}BaCo_2O_{5.5}$, stabilization of AFM phase by hydrostatic pressure is confirmed by even higher values of pressure coefficients for T_N and T_C [$dT_C/dP = -1.11(8)$ K/kbar, $dT_N/dP = 5.35(95)$ K/kbar]. For larger hole doping of $Nd_{0.94}Ca_{0.06}BaCo_2O_{5.5}$ up to $\delta = 0.54$ ($c = 0.10$) [Fig. 6(a), lower panel)], the antiferromagnetic phase was not induced under pressure and T_C showed a minor decrease [$dT_C/dP = -0.11(9)$ K/kbar].

Figure 6(b) presents magnetic hysteresis loops measured at 150 K under ambient and hydrostatic pressure for $Nd_{0.94}Ca_{0.06}BaCo_2O_{5+\delta}$. All clearly visible hysteresis loops at ambient pressure are characteristic of hard magnetic materials, which are suppressed under pressure for $\delta = 0.42$ and 0.49. For $\delta = 0.52$ (not shown) and 0.54 [lower panel of Fig. 6(b)], which are fully ferrimagnetic, the pressure impact on magnetism is much smaller. Additionally, the loop for $\delta = 0.52$ (not shown) reveals a concavity effect similar to that observed in invar alloys [23]. When the antiferromagnetic phase is absent, an increase of magnetization below T_C is seen, indicating enhancement of the ferrimagnetic phase under pressure (see the lower panel of Fig. 6(a) and Ref. [11]). Such a behavior of T_C under pressure for all investigated samples of $Nd_{0.94}Ca_{0.06}BaCo_2O_{5+\delta}$ supports the idea of the usual ferromagnetic phase created by Co^{3+}/Co^{4+} paths, which exhibits a tendency to a small decrease of T_C with increasing pressure [10,18]. This seems to be remarkable, in particular for $Nd_{0.94}Ca_{0.06}BaCo_2O_{5.42}$, in which ferrimagnetism is mainly dominated by Co^{2+}/Co^{3+} paths. Obviously, this does not exclude the possibility of charge disproportion of Co^{3+} ions to Co^{2+} and Co^{4+} [17] and/or spin-state transitions, since the electron doping of this compound is not so significant ($c = -0.05$). In order to compare these observations, we have performed magnetic studies for $Nd_{0.9}Ca_{0.1}Co_2O_{5+\delta}$, i.e., the family of compounds in which perfectly ordered composition ($\delta = 0.5$, $c = 0.05$) is fully ferrimagnetic.

F. Magnetic properties of $Nd_{0.9}Ca_{0.1}BaCo_2O_{5+\delta}$

Figure 7(a) presents the $M(T)$ dependences for $Nd_{0.9}Ca_{0.1}BaCo_2O_{5+\delta}$ with $\delta = 0.07$–0.76. The characteristic

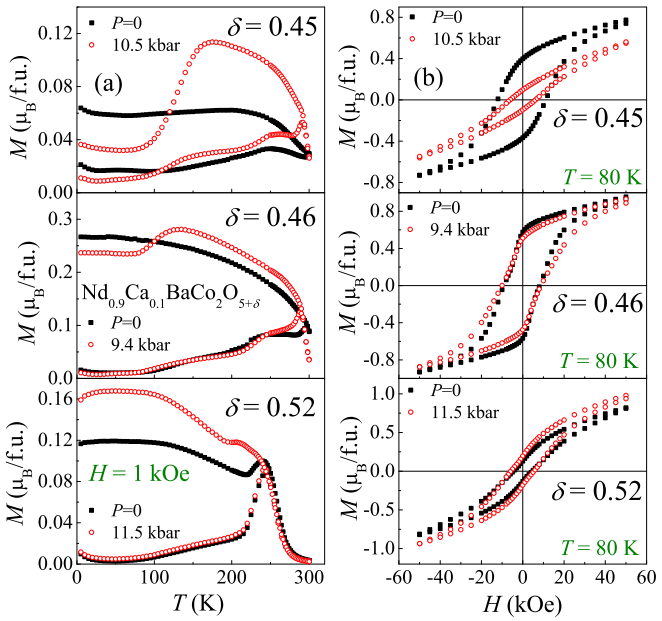

FIG. 8. (a) Temperature dependences of ZFC and FC magnetization of $Nd_{0.9}Ca_{0.1}BaCo_2O_{5+\delta}$ measured at 1 kOe for selected δ index at ambient and under hydrostatic pressure. (b) Magnetic field dependences of magnetization for $Nd_{0.9}Ca_{0.1}BaCo_2O_{5+\delta}$ for selected oxygen contents, measured using the FC procedure in 50 kOe at ambient and under hydrostatic pressure.

temperatures determined from the $M(T)$ curve are presented in Fig. 7(b). We have shown previously that the AFM phase is completely suppressed for $\delta = 0.5$ [5] and the same is observed for $0.45 < \delta < 0.51$ [Figs. 7(a) and 7(b)]. However, a slight increase of δ up to 0.52 resulted in the emergence of the antiferromagnetic phase, evidenced by the cusp of $M(T)$ at ~ 240 K, which separates the ferrimagnetic-to-paramagnetic transition at T_C (= 246 K) from the AFM-to-ferrimagnetic transition at T_N (= 230 K). A divergence between ZFC and FC curves at around T_N, similar to that observed for $\delta = 0.54$ [see the lower panel of Fig. 6(a)], confirmed the δ-induced first-order magnetic-phase transition from AFM to ferrimagnetic state. This phenomenon is accompanied by a huge decrease of magnetization when compared to the sample with $\delta = 0.51$ and a large decrease of T_C. These observations are remarkable for the hole-doped composition ($c = 0.07$) with dominant ferromagnetic interactions of Co^{3+}/Co^{4+}. They cannot be correlated with the changes in crystal structure since no structural phase transitions have been found [Fig. 2(d)]. However, they are clearly present in the $Nd_{1-x}Ca_xBaCo_2O_{5+\delta}$ system since the absence of the AFM phase is observed for $Nd_{0.94}Ca_{0.06}BaCo_2O_{5.52}$ and $Nd_{0.9}Ca_{0.1}BaCo_2O_{5.5}$, both with $c = 0.05$.

G. Pressure dependence of magnetic properties of $Nd_{0.9}Ca_{0.1}BaCo_2O_{5+\delta}$

Figure 8(a) presents the $M(T)$ dependences of magnetization of $Nd_{0.9}Ca_{0.1}BaCo_2O_{5+\delta}$ under ambient and under hydrostatic pressure for selected δ values within the orthorhombic structure. As discussed previously, the T_C decreases under pressure for $Nd_{1-x}Ca_xBaCo_2O_{5.5}$ for increasing $x = 0$–0.1 [10]. The same is observed for $x = 0.1$ and $\delta = 0.52$ [lower panel of Fig. 8(a), $dT_C/dP = -0.35(10)$ K/kbar] and surprisingly the AFM phase is also suppressed under pressure. For $\delta = 0.45$ and 0.46 ($c \sim 0$), the tendency to decrease of T_C with pressure is preserved [upper and middle panels of Fig. 8(a)]. However, because of limitations of temperature measurements, the dT_C/dP coefficients were not derived for these samples. At lower temperatures, the pressure-induced phase transition to AFM phase can be observed, more pronounced for $\delta = 0.45$ than for 0.46. In order to confirm this finding, the measurements of magnetic-field hysteresis were performed at 80 K, i.e., the temperature at which the AFM phase should be observed under pressure for both $\delta = 0.45$ and 0.46. Indeed, the results shown in Fig. 8(b) demonstrate for $\delta = 0.45$ the strong suppression of magnetization, confirming transition to the AFM state. Somewhat smaller suppression is observed for the sample with $\delta = 0.46$, which is in an agreement with $M(T)$ dependence [upper panel of Fig. 8(a)] Thus, similarly as for $x = 0.06$ composition, all the registered loops are characteristic of hard magnetic materials but are in contrast to the $NdBa_{1-y}La_yCo_2O_{5+\delta}$ compositions for which rather weak hysteresis loops were observed (see insets of Fig. 4).

H. Phase diagram of $Nd_{1-x}Ca_xBa_{1-y}La_yCo_2O_{5+\delta}$

Figure 9(a) presents the phase diagram for the whole investigated system $Nd_{1-x}Ca_xBa_{1-y}La_yCo_2O_{5+\delta}$ with fixed $\delta = 0.5$. Variation of transition temperatures T_C, T_N, and T_{MIT} with charge-doping level $c = (x-y)/2 + \delta - 0.5$ was determined from dc magnetic measurements. The effect of increasing c on transition temperatures is noticeably different: the T_C increases over the whole range of c, the T_N has maximum at $c = 0$, while T_{MIT} remains practically unchanged. The application of hydrostatic pressure of ~ 9.5 kbar slightly suppresses T_C and increases T_N, especially for $c < 0$, by stabilization of the AFM phase.

Expanding observations of transition temperatures behavior to other oxygen concentrations retaining ordered orthorhombic phase [see Fig. 2(e)], it is revealed [Fig. 9(b)] that the value of T_C clearly decreases with an increase of δ for both the Ba- and Nd-site substitutions, and that the value of T_C is lower for the compounds substituted at the Ba site. Figure 9(c) shows the changes of T_N, which indicate that the AFM phase is suppressed for Nd-Ca substitution and exists in a narrower range of oxygen compositions than the ferro(ferri)magnetic phase [Fig. 9(a)], For the Ba-La substitution, both anti- and ferro(ferri)magnetic phases are observed to coexist.

The complex investigation of structural, magnetic, and electronic properties of the heterovalent Nd- and Ba-substituted $Nd_{1-x}Ca_xBa_{1-y}La_yCo_2O_{5+\delta}$ system over a wide range of oxygen content ($0.07 < \delta < 0.84$) has revealed interesting features that may involve further work in order to fully resolve the origin of the complex magnetic and electronic behavior by inclusion of local structural parameters as a function of charge doping, oxygen disorder, and pressure. In this work, the observed properties have been related to the charge doping $c = (x-y)/2 + \delta - 0.5$ and the disturbance of the perfect oxygen vacancy ordering present at $\delta = 0.5$. The key observation of the present study is that gradual enhancement of T_C is observed

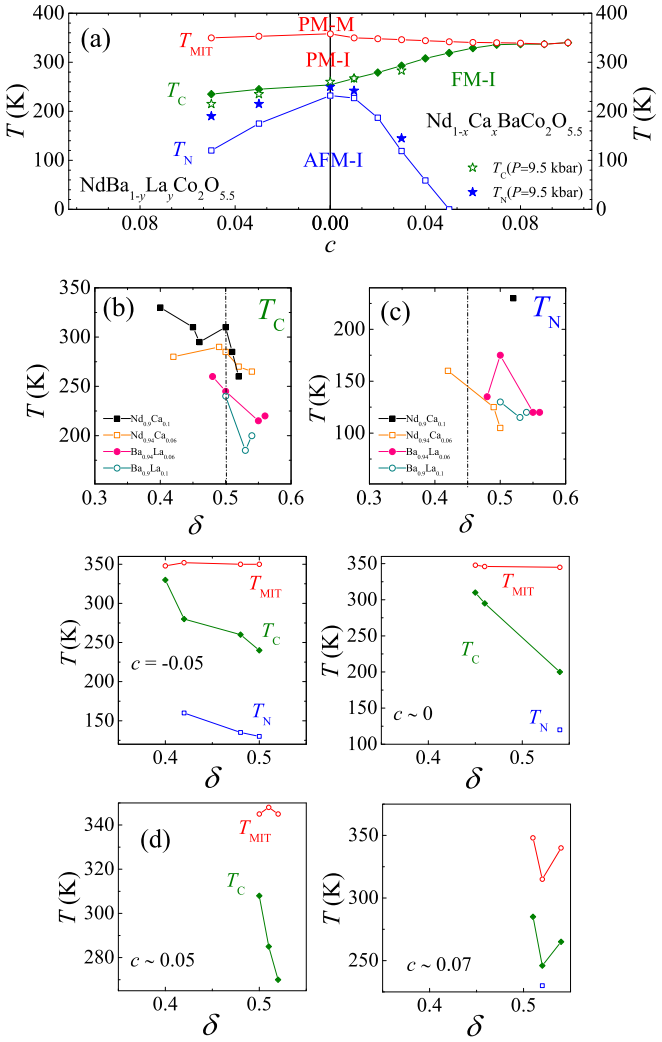

FIG. 9. (a) Phase diagram of (Nd,Ca)(Ba,La)$Co_2O_{5+\delta}$, in which PM-M is the paramagnetic metallic phase, PM-I is the paramagnetic insulating phase, FM-I is the ferrimagnetic insulating phase, and AFM-I is the antiferromagnetic insulating phase. The main transition temperatures T_N, T_C, and T_{MIT} are plotted. Panel (b) shows oxygen content dependence of T_C for (Nd,Ca)(Ba,La)$Co_2O_{5+\delta}$. Panel (c) shows oxygen content dependence of T_N for (Nd,Ca)(Ba,La)$Co_2O_{5+\delta}$. Panel (d) shows δ dependence of main transition temperatures at fixed selected values of carrier doping parameter c.

over the whole range of c, unaffected by oxygen vacancy disorder.

The T_N has a maximum at $c = 0$ for parent composition $NdBaCo_2O_{5.5}$ and it does not fall to zero for $NdBa_{0.9}La_{0.1}Co_2O_{5.5}$ ($c = -0.05$) when compared to corresponding Ca/Nd substitution with $c = 0.05$, indicating that oxygen vacancy disorder, especially for $\delta > 0.5$, has a larger effect on the AFM phase than the charge doping. The importance of oxygen disorder is observed in the case of T_C and T_N for $Nd_{1-x}Ca_xBaCo_2O_{5+\delta}$, for both x equal to 0.06 and 0.10. In the case of $Nd_{0.94}Ca_{0.06}BaCo_2O_{5+\delta}$, with $-0.05 < c < 0.07$, the hole doping up to 0.07 by oxygen addition lowers T_C, while it is increased by the equivalent hole doping of Ca/Nd substitution of $NdBaCo_2O_{5.5}$. For $Nd_{0.9}Ca_{0.1}BaCo_2O_{5.52}$, we have found the δ-induced first-order magnetic-phase transition from AFM to ferrimagnetic state. This transition is accompanied by a huge decrease of magnetization when compared to the sample with $\delta = 0.51$ and large decrease of T_C.

Complex magnetic behavior was strongly affected by hydrostatic pressure, which we have attempted to explain by ferro- and antiferromagnetic interactions resulting from charge separation and spin transitions. For all investigated slightly electron-doped samples of La/Ba substitution, with $-0.05 < c < 0.01$, we observe strong suppression of the ferrimagnetic state under pressure at the cost of the AFM one, evidenced by a striking decrease of magnetization, as well as by the large value of pressure coefficient: $dT_N/dP = 5.75$ K/kbar. When the antiferromagnetic phase is absent, as for $Nd_{0.94}Ca_{0.06}BaCo_2O_{5.54}$, an enhancement of ferrimagnetic phase under pressure is observed. For $Nd_{0.9}Ca_{0.1}BaCo_2O_{5.52}$, the AFM phase, induced under ambient pressure by δ variation, is suppressed under pressure. For $\delta = 0.45$ and 0.46, we have observed the pressure-induced phase transition to AFM phase.

IV. CONCLUSIONS

We have studied the evolution of magnetic and electronic phases of the heterovalent Nd- and Ba-substituted $Nd_{1-x}Ca_xBa_{1-y}La_yCo_2O_{5+\delta}$ system over a wide range of oxygen content ($0.07 < \delta < 0.84$). Single-phase oxygen-ordered orthorhombic phase exhibiting complex phase transitions was found for $x \leqslant 0.2$ and $y \leqslant 0.1$ for a narrow oxygen range around $\delta = 0.5$, as shown in Fig. 2(e). The observed properties have been related to the charge doping $c = (x-y)/2 + \delta - 0.5$ and the disturbance of the perfect oxygen vacancy ordering present at $\delta = 0.5$. Gradual enhancement of T_C was observed over the whole range of c, unaffected by oxygen vacancy disorder. The T_N has a maximum at $c = 0$ and rapidly disappears for $c = 0.05$ for Ca/Nd substitution while it is maintained for La/Ba, indicating that oxygen vacancy disorder, especially for $\delta > 0.5$, has a larger effect on the AMF phase than the charge doping. The T_{MIT} was found practically unchanged, unaffected by either charge doping or disorder. The application of hydrostatic pressure slightly suppressed T_C and increased T_N by stabilization of the AFM phase with a largest value of $dT_N/dP = 5.75$ K/kbar.

Complex magnetic behavior was strongly affected by hydrostatic pressure, which we have attempted to explain by ferro- and antiferromagnetic interactions resulting from charge separation and spin transitions. However, the complexity of the system with four spin-ordered Co sites below T_{MIT}, which are in addition affected by varying the oxygen contents, does not make this explanation unique. Further work would be required to fully resolve the origin of the complex magnetic and electronic behavior by inclusion of local structural parameters as a function of charge doping, oxygen disorder, and pressure.

ACKNOWLEDGMENT

This work was supported by National Science Centre (Poland) under Contract No. 1662/B/H03/2011/40.

[1] C. Martin, A. Maignan, D. Pelloquin, N. Nguyen, and B. Raveau, Appl. Phys. Lett. **71**, 1421 (1997).
[2] D. Akahoshi and Y. Ueda, J. Solid State Chem. **156**, 355 (2001).
[3] A. Maignan, C. Martin, D. Pelloquin, N. Nguyen, and B. Raveau, J. Solid State Chem. **142**, 247 (1999).
[4] A. A. Taskin, A. N. Lavrov, and Y. Ando, Phys. Rev. B **71**, 134414 (2005).
[5] S. Kolesnik, B. Dabrowski, O. Chmaissem, S. Avci, J. P. Hodges, M. Avdeev, and K. Swierczek, Phys. Rev. B **86**, 064434 (2012).
[6] P. Miao, X. Lin, S. Lee, Y. Ishikawa, S. Torii, M. Yonemura, T. Ueno, N. Inami, K. Ono, Y. Wang, and T. Kamiyama, Phys. Rev. B **95**, 125123 (2017).
[7] G. Aurelio, J. Curiale, R. D. Sanchez, and G. J. Cuello, Phys. Rev. B **76**, 214417 (2007).
[8] A. Bharathi, P. Yasodha, N. Gayathri, A. T. Satya, R. Nagendran, N. Thirumurugan, C. S. Sundar, and Y. Hariharan, Phys. Rev. B **77**, 085113 (2008).
[9] Y.-K. Tang and C. C. Almasan, Phys. Rev. B **77**, 094403 (2008).
[10] J. Pietosa, A. Szewczyk, R. Puzniak, A. Wisniewski, B. Dabrowski, and S. Kolesnik, J. Appl. Phys. **116**, 013903 (2014).
[11] J. Pietosa, S. Kolesnik, R. Puzniak, and B. Dabrowski, Acta Phys. Pol. A **126**, A-50 (2014).
[12] J. Pietosa, K. Piotrowski, R. Puzniak, A. Wisniewski, S. Kolesnik, and B. Dabrowski, J. Alloys Compd. **645**, 223 (2015).
[13] K. Murata, H. Yoshino, H. O. Yadav, Y. Honda, and N. Shirakava, Rev. Sci. Instrum. **68**, 2490 (1997).
[14] J. Kamarad, A. Machatova, and Z. Arnold, Rev. Sci. Instrum. **75**, 5022 (2004).
[15] A. A. Taskin, A. N. Lavrov, and Y. Ando, Phys. Rev. B **73**, 121101(R) (2006).
[16] G. Aurelio, J. Curiale, R. D. Sanchez, and G. J. Cuello, Physica B **398**, 223 (2007).
[17] M. M. Seikh, V. Caignaert, V. Pralong, Ch. Simon, and B. Raveau, J. Phys.: Condens. Matter. **20**, 015212 (2008).
[18] M. M. Seikh, B. Raveau, V. Caignaert, and V. Pralong, J. Magn. Magn. Mater. **320**, 2676 (2008).
[19] N. Thirumurugan, A. Bharathi, A. Arulraj, and C. S. Sundar, Mater. Res. Bull. **47**, 941 (2012).
[20] J. B. Goodenough, *Magnetism and the Chemical Bond* (Wiley Interscience, New York, 1963).
[21] X. Zhang, X.-M. Wang, H.-W. Wie, X.-H. Lin, Ch.-H. Wang, Y. Zhang, Ch. Chen, and X.-P. Jing, Mater. Res. Bull. **65**, 80 (2015).
[22] M. M. Seikh, C. Simon, V. Caignaert, V. Pralong, M. B. Lepetit, S. Boudin, and B. Raveau, Chem. Mater. **20**, 231 (2008).
[23] A. H. Morrish, *Physical Principles of Magnetism* (John Wiley and Sons, New York, 1965).